Novel Regiospecific MDMO−PPV Copolymer with Improved Charge Transport for Bulk Heterojunction Solar Cells

Attila J. Mozer,*,†,‡ Patrick Denk,† Markus C. Scharber,† Helmut Neugebauer,‡ and N. Serdar Sariciftci‡

Forschungs- und Entwicklungs GmbH, Konarka Austria, Gruberstrasse 40−42, A-4020 Linz, Austria, and Linz Institute for Organic Solar Cells (LIOS) Physical Chemistry, Johannes Kepler University Linz, Altenbergerstrasse 69, A-4040 Linz, Austria

Pawel Wagner,§ Laurence Lutsen,|| and Dirk Vanderzande§,||

Organic and Polymer Chemistry Group, Limburgs Universitaire Centrum (LUC), Diepenbeek, B-3590, Belgium, and IMOMEC Division, Organic and Polymer Chemistry Group, IMEC, Wetenschapspark 1, Diepenbeek, B-3590, Belgium

Received: January 7, 2004; In Final Form: February 26, 2004

A novel regiospecific MDMO−PPV copolymer has been synthesized by the copolymerization of the mixture of 70 wt % 1-(chloromethyl)-5-[(3,7-dimethyloctyl)oxy]-2-methoxy-4-[(octylsulfoxy)methyl]benzene (monomer A) and 30 wt % 1-(chloromethyl)-2-[(3,7-dimethyloctyl)oxy]-5-methoxy-4-[(octylsulfoxy)methyl]benzene (monomer B) via the sulfinyl precoursor synthetic route. The hole mobility of the new regiospecific MDMO−PPV polymer (also called OC**1**C**10**−PPV) measured with a time-of-flight setup is found to be a factor of ∼3.5 higher at all measured electric fields at room temperature as compared to regiorandom MDMO−PPV. The electric field and temperature dependence of the hole mobility is discussed in the framework of disorder formalism. The improved charge transport properties of the novel regiospecific MDMO−PPV copolymer is attributed to the better interchain interactions facilitated by the more regular PPV backbone, which is also supported by the red shifted optical absorption and photoluminescence. Finally, the improved charge transport properties have been utilized by the fabrication of bulk heterojunction photovoltaic devices with a very high (0.71) filling factor based on the blend of the novel regiospecific MDMO−PPV copolymer and the soluble fullerene derivative 1-[3-(methoxycarbonyl)propyl]-1-phenyl-(6,6)-C_{61} (PCBM).

1. Introduction

The need for renewable and inexpensive photovoltaic energy inspires organic photovoltaic research. One of the most promising approaches consists of the blend of a strongly light absorbing conjugated semiconducting polymer and a soluble fullerene derivative deposited onto a transparent conductive substrate by simple solution processing technique.[1] Such "bulk heterojunction" solar cells based on the blends of poly{[2-methoxy-5-[(3,7-dimethyloctyl)oxy]phenylene]vinylene} (MDMO−PPV) and 1-[3-(methoxycarbonyl)propyl]-1-phenyl-(6,6)-C_{61} (PCBM) have been fabricated and extensively studied with power conversion efficiencies up to 3%.[2−4] One of the important parameters is the charge carrier mobility in the bulk heterojunction solar cells.[5,6] Recently it was reported from space charge limited current measurements that the electron mobility of pristine PCBM thin films ($\mu_e = 2 \times 10^{-3}$ cm^2 V^{-1} s^{-1}) is several orders of magnitude higher than the hole mobility of pristine MDMO−PPV thin films ($\mu_h = 5 \times 10^{-7}$ cm^2 V^{-1} s^{-1}).[7] Although the electron and hole mobility of the interpenetrating phases of the MDMO−PPV:PCBM blend might differ from the values of the pristine, individual components,[6] the above study suggests that in order to achieve improved and balanced charge transport, the intrinsic hole transport properties of MDMO−PPV needs to be improved.

A promising strategy for enhancing the charge carrier mobility of conjugated polymers is the synthesis of regioregular polymers (as demonstrated in poly(3-hexylthiophene) compared to the regiorandom counterpart).[8,9] The highest charge carrier mobility of conjugated polymers reported so far in the literature was determined in highly regioregular and ordered films of poly(3-hexylthiophene) produced by a structure-controlled synthesis.[9] A novel synthetic route to MDMO−PPV based on the nonionic polymerization of the 50:50 wt % mixture of the asymmetrically substituted stereoisomer monomers of the sulfinyl precoursor route has been recently published by Lutsen et al.[10] It was reported that the polymerization of only one of the pure monomer isomers leads to a practically insoluble regioregular homopolymer. Unfortunately, insolubility prevents otherwise promising substances from practical use in photovoltaic devices based on solution deposition techniques.

In the present work, we synthesized a novel soluble, regiospecific MDMO−PPV copolymer by the copolymerization of a mixture of 70 wt % 1-(chloromethyl)-5-[(3,7-dimethyloctyl)oxy]-2-methoxy-4-[(octylsulfoxy)methyl]benzene (monomer A) and 30 wt % 1-(chloromethyl)-2-[(3,7-dimethyloctyl)oxy]-5-methoxy-4-[(octylsulfoxy)methyl]benzene (monomer B) via

* Corresponding author. Fax: +43-732-2468-8770. E-mail: attila.mozer@jku.at.
† Konarka Austria.
‡ Johannes Kepler University Linz.
§ Limburgs Universitaire Centrum (LUC).
|| IMEC.

10.1021/jp049918t CCC: $27.50 © 2004 American Chemical Society
Published on Web 04/02/2004

SCHEME 1: Synthesis of the MDMO−PPV Copolymers

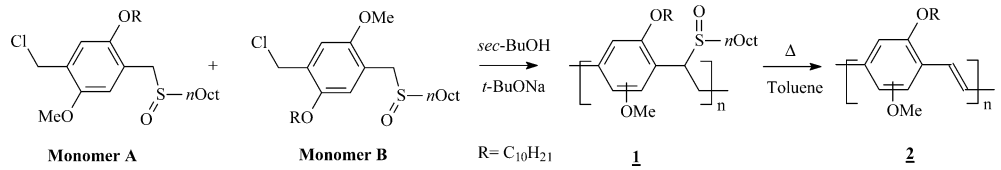

the sulfinyl precoursor synthetic route. The charge carrier mobility of the novel regiospecific MDMO−PPV copolymer at various temperatures and electric fields with a time-of-flight technique is studied. It was found that the charge carrier mobility at room temperature is enhanced as the regioregularity of the MDMO−PPV is increased. Moreover, by analyzing the temperature and electric field dependence of the charge carrier mobility in the framework of disorder formalism,[11] we discuss the "molecular structure−charge transport property" correlation in these conjugated polymers. Finally, we prepared bulk heterojunction solar cells based on this novel regiospecific MDMO−PPV copolymer and obtained high efficiencies and unusually high filling factors.

2. Disorder Formalism

Charge carrier mobility in amorphous conjugated polymers is generally orders of magnitude lower (10^{-3} to 10^{-8} cm^2 V^{-1} s^{-1}) and strongly temperature and electric field dependent in contrast to organic single crystals ($\sim 10^1$ to 10^{-1} cm^2 V^{-1} s^{-1}).[12] Although the on-chain charge carrier mobility in conjugated polymers determined by microwave conductivity experiments[13,14] reaches that of crystalline organic solids, the macroscopic charge transport properties in amorphous films are controlled by interchain hopping processes.[15] Among the several models available in the literature,[16] disorder formalism developed by Bässler and co-workers[11] has been the most widely employed to describe the peculiar nature of charge transport in molecularly doped polymers,[16] molecular glasses,[17] and particularly conjugated polymers.[18,19] The model uses the notion that both the energy levels and the intersite distance of the transport sites are subject to a distribution in an amorphous solid medium. The authors of the theory assume a Gaussian distribution for both the energetic and the positional disorder supported by the fact that the absorption profiles of disordered materials generally feature Gaussian line shapes. Monte Carlo simulations for hopping transport using Miller−Abrahams form of hopping rate[20] within a Gaussian distribution of localized states results in eq 1.[11]

$$\mu(\hat{\sigma},\Sigma, E) = \mu_0 \exp\left[-\left(\frac{2}{3}\hat{\sigma}\right)^2\right] \begin{cases} \exp[C(\hat{\sigma}^2 - \sum^2)E^{1/2}] & (\sum \geq 1.5) \\ \exp[C(\hat{\sigma}^2 - 2.25)E^{1/2}] & (\sum < 1.5) \end{cases} \quad \text{(A1)}$$

where $\hat{\sigma} = \sigma/(kT)$ and Σ are parameters characterizing energetic disorder and positional disorder, respectively, σ (eV) is the width of the Gaussian density of states, μ_0 (cm^2 V^{-1} s^{-1}) is a prefactor mobility in the energetic disorder-free system, E (V cm^{-1}) is the electric field, and $C = 2.9 \times 10^{-4}$ [(cm V^{-1})$^{1/2}$] is a fit parameter. In a refinement, C was related to the electric field dependence of the mobility.[18] According to the model, the logarithm of the charge carrier mobility is proportional to the square root of the electric field, and inversely proportional to the square of temperature.

3. Experimental Section

3.1. Synthesis of the MDMO−PPV Copolymers. *Synthesis of the Stereoisomer Monomers 1-(Chloromethyl)-5-[(3,7-dimethyloctyl)oxy]-2-methoxy-4-[(octylsulfoxy)methyl]benzene (Monomer A) and 1-(Chloromethyl)-2-[(3,7-dimethyloctyl)oxy]-5-methoxy-4-[(octylsulfoxy)methyl]benzene (Monomer B) (See Scheme 1).* The synthesis of the mixture of the asymmetric monomer isomers was performed following the synthethic procedure descibed elsewhere.[21,22] The mixture was separated on a chromatographic column (silica gel, hexane:ethyl acetate 1:1) to obtain the two isomers. Each fraction was further purified on a chromatographic column (silica gel, gradient concentration of ethyl acetate in hexane from pure hexane to 40% of ethyl acetate).

1-(Chloromethyl)-5-[(3,7-dimethyloctyl)oxy]-2-methoxy-4-[(octylsulfoxy)methyl]benzene (monomer A) was obtained as colorless or light yellow viscous oil, solidified at low temperature (−19 °C) to white crystals.

1-(Chloromethyl)-2-[(3,7-dimethyloctyl)oxy]-5-methoxy-4-[(octylsulfoxy)methyl]benzene (monomer B) was obtained as colorless or pale yellow-green viscous oil, solidified at room temperature to white crystals.

Synthesis of the Precursor Polymers. A solution of 0.97 g (2 mmol) of the mixture of monomer A and monomer B (or only the pure monomers) in 14 mL of *sec*-butanol and a solution of 0.25 g (2.6 mmol) of sodium *tert*-butoxide in 10 mL of *sec*-butanol was flushed with nitrogen for 1 h at 30 °C. The solution of *tert*-butoxide was added in one portion to the stirred monomer solution. After 1 h, the reaction mixture was poured into 200 mL of well-stirred ice-cold water.

The part insoluble in water was dissolved in 50−100 mL of chloroform, dried over magnesium sulfate, and evaporated under vacuum at 60 °C. Then the solid was redissolved in 8 mL of chloroform and precipitated in 170 mL of ice-cold methanol. Methanol was decanted, and the main fraction of precursor polymer I (see Table 1S) was obtained. Then the decanted methanol fraction was evaporated in a vacuum at 60 °C to dryness, and the resulting solid was washed three times by methanol. The insoluble part was dried in a vacuum overnight and fraction II of polymerization was obtained. The decanted methanol from the second step was evaporated in a vacuum at 60 °C to dryness and fraction III was obtained.

Fractions I and II (see **1** in Scheme 1) are the polymer fractions; meanwhile, fraction III contains only oligomers (Table 1S).

Conversion of the Precursor Polymers. The precursor polymer fractions I and II were mixed and dissolved in toluene (100 mg of precursor polymer in 10 mL of toluene). The resulting

TABLE 1: Determined Values of μ_{RT} (Room-Temperature Mobility), and Parameters μ_0 (Prefactor Mobility), σ (Energetic Disorder), and C (Field Dependence of μ) of the Disorder Formalism (Eq 1)

sample[a]	μ_{RT} (cm^2 V^{-1}s^{-1})[b]	μ_0 (cm^2 V^{-1} s^{-1})	σ (meV)	C [(cm V^{-2})$^{1/2}$]
1	2.8×10^{-5}	2.6×10^{-3}	115	1.54×10^{-4}
2	0.85×10^{-5}	0.22×10^{-3}	105	1.35×10^{-4}

[a] Samples 1 and 2 stand for 70:30 RS-MDMO−PPV and RRa-MDMO−PPV, respectively. [b] Room-temperature mobility was measured at ~300 K and 5×10^5 V cm^{-1} electric field.

light green solution was flushed with nitrogen at room temperature for 1 h. Then the reaction mixture was refluxed for 3 h under nitrogen atmosphere during which time the elimination of the sulfinyl group resulted in conversion to the conjugated polymer (see **2** in Scheme 1). The resulting red solution was evaporated to dryness under reduced pressure at 80 °C, dissolved in hot chloroform or chlorobenzene (usually 80−100 mL), and precipitated by 150 mL of methanol. The resulting red solid was isolated by filtration and washed twice with 20 mL of methanol.

Regiorandom MDMO−PPV was purchased from Covion GmbH. PCBM was provided by J. C. Hummelen from Rijksuniversiteit Groningen.

3.2. Experimental Setups and Sample Preparation. *UV−Vis Absorption and Photoluminescence (PL).* UV−vis absorption spectra in dilute chlorobenzene solutions were recorded by a HP 8453 UV−Visible System. Thin film samples for the PL were prepared by the doctor blade technique from 1 wt % chlorobenzene solution onto microscope slides as substrates. PL of the thin film samples was measured as follows: The samples were mounted into a cryostat and placed in the focus of a 5 cm diameter collecting lens. The samples were illuminated from the front side by the 514 nm line of an Ar^+ laser with 0.3 mW intensity. A lowpass filter was used to block the Ar^+ excitation line, and the collected light was coupled to an optical fiber, dispersed by a $L = {}^1/_8$ m monochromator and detected by a Si photodetector array. Three different spots have been measured for each sample. The spectral resolution of the setup was determined from the full width at half-maximum of the Ar^+ ion excitation line to be 1 nm.

Time-of-Flight (ToF) Mobility Measurement Setup. Typically, 1−2 μm thick films were prepared by the doctor blade technique from 1 wt % chlorobenzene solution onto structured ITO coated glass substrates. On top, Al was evaporated as cathode in a vacuum better than 10^{-5} mbar (Al layer thickness 80 nm). The samples were illuminated from the ITO side using the second harmonic (532 nm) of a Nd:YAG pulsed laser (Coherent Infinity 40−100). The photogenerated charges drifted through the sample under the external electric field applied by a Brandenberg 477−303 voltage supply and were recorded by a Tektronix TDS 754 C Digitizing Oscilloscope using a Femto DLPCA low noise current amplifier. The transit time of charge carriers did not change significantly upon changing the incoming light intensity by using optical density filters up to OD 3, which indicates that the determined transit times were a true measure of the transit time of the photogenerated charge carriers and space charge effects are negligible.

From the applied bias and the sign of the photocurrent it is evident that the drifting charges were holes. The photocurrent transients typically show a narrow plateau region and a broad dispersive tail as has been shown earlier for several PPV derivatives.[19,23] The time-of-flight (ToF) mobility was calculated from the transit time of charge carriers as $\mu = d^2/(Vt_{tr})$, where μ ($cm^2\ V^{-1}\ s^{-1}$) is the mobility, d (cm) is the film thickness, V (V) is the applied potential, and t_{tr} (s) is the transit time of charge carriers. The transit time of charge carriers was defined as the meeting point of the asymptotes of the two linear regimes in the log photocurrent vs log time plots.[16] More than 10 devices with varying active layer thickness were measured for both MDMO−PPV samples. The temperature dependence measurements were performed using a temperature-controlled liquid nitrogen cooled cryostat (Oxford Optistat DN-V, ITC 503 temperature controller, precision ±0.1 K). The temperature dependence of mobility was determined for at least 2 samples of each material. The thickness of the films was determined using a Tencor Instruments Alphastep Semiconductor Profiler.

Photovoltaic Devices (PV). PV devices were made of a layered structure of indium tin oxide (ITO)/PEDOT [poly(3,4-ethylenedioxythiophene)−poly(styrenesulfonate)]/MDMO−PPV:PCBM (1:4)/LiF/Al, following the procedure described elsewhere.[1] All the PV devices were prepared and measured in an argon atmosphere dry glovebox. The current voltage characteristics were recorded with a Keithley SMU 2400 unit. The devices were illuminated from the transparent ITO side using a Steuernagel solar simulator simulating the AM (air mass) 1.5 sun spectrum. The power conversion efficiency of the solar cells under simulated AM 1.5 conditions were calculated as

$$\eta_{AM1.5}\,(\%) = \left(\frac{P_{out}m}{P_{in}}\right) \times 100 = \frac{\mathrm{FF}\ V_{oc}J_{sc}m}{P_{in}} \times 100 \quad \text{(A.2)}$$

where P_{out} (mW cm^{-2}) is the output electrical power of the device under illumination, P_{in} (mW cm^{-2}) is the light intensity incident on the sample as measured by a calibrated photodiode, and m is the spectral mismatch factor[24] that accounts for deviations in the spectral response to that of the reference cell. Furthermore, FF is the filling factor defined as

$$\mathrm{FF} = \frac{V_{mpp}J_{mpp}}{V_{oc}J_{sc}} \quad \text{(A3)}$$

where V_{mpp} (V) and J_{mpp} (mA cm^{-2}) are the maximum voltage and maximum current density at the maximum power point, respectively, V_{oc} (V) is the open-circuit voltage, J_{sc} (mA cm^{-2}) is the short-circuit current density. The incoming light intensity was 80 mW cm^{-2} during the experiments, and the spectral mismatch factor was 0.753.

Results and Discussion

4.1. Properties of the MDMO−PPV Copolymers. Detailed information on the general properties of the MDMO−PPV copolymers, including the weight averaged molecular weights and polymerization yields, is provided in the Supporting Information Table 1S. Suffice to mention here that as the weight percent of either one of the isomer monomers is increased in the reaction mixture above 80%, an additional absorption feature appears at wavelengths longer than the band gap absorption of the isolated conjugated chain, (indicated with an arrow in Figure 1A), which is attributed to aggregate formation in solution. In addition, the absorption maximum of the conjugated polymers is red shifted as the weight percent of either one of the monomers is increased (Figure 1B), which is indicative of longer effective conjugation length attributed to the enhanced regioregularity of the conjugated backbone. Because the preparation of bulk heterojunction photovoltaic devices requires a well soluble conjugated polymer, we have chosen the conjugated polymer resulting from the polymerization of the 70:30 wt % mixture of monomer A and monomer B (referred to as "70:30 RS-MDMO−PPV") and compare its charge transport and photovoltaic properties to the regiorandom MDMO−PPV (referred to as "RRa-MDMO−PPV") purchased from Covion GmbH.

4.2. Charge Carrier Mobility. The room-temperature electric field dependent ToF mobility of 70:30 RS-MDMO−PPV is compared to RRa-MDMO−PPV in Figure 2 for several films with varying thickness (0.32−2.3 μm). The mobility follows the form $\log \mu \propto E^{1/2}$ for both polymers, a behavior frequently observed for a wide range of disordered organic semiconductors[16] and described in the disorder model illustrated in section

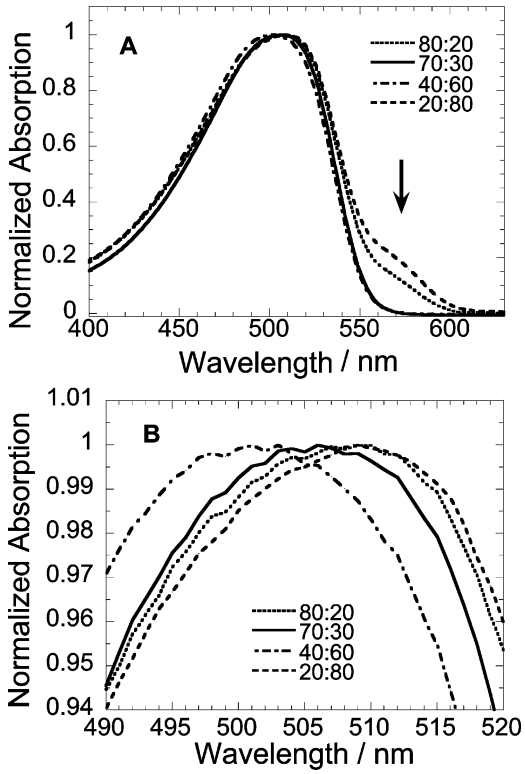

Figure 1. (A) Absorption spectra of selected MDMO−PPV copolymers in dilute chloroform solution. (B) Absorption spectra of selected MDMO−PPV copolymers in dilute chloroform solution showing the region near the peak of the absorption maximum for better comparison.

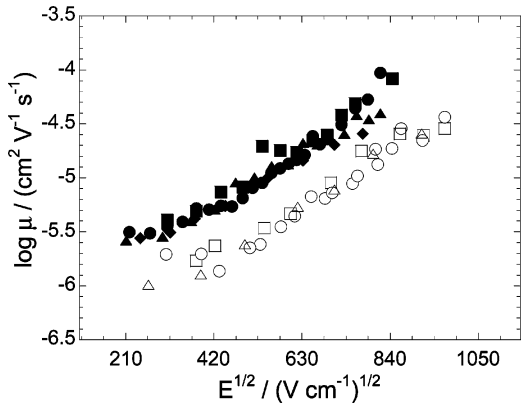

Figure 2. Comparison of the field dependent room-temperature mobility of 70:30 RS-MDMO−PPV (full symbols) and RRa-MDMO−PPV (empty symbols) for various sample thicknesses: (●) 2.1 μm; (■) 1.05 μm; (▲) 0.5 μm; (▼) 0.45 μm; (○) 2.3 μm; (□) 1.68 μm; (△) 1.72 μm; (▽) 0.32 μm.

2. The room-temperature mobility of 70:30 RS-MDMO−PPV is approximately 3.5 times larger at all measured electric fields for all film thicknesses as compared to the RRa-MDMO−PPV. It is interesting to note that although the shape of the photocurrent transients became more dispersive as the thickness of the samples decreased (see Figure 3), we did not observe a significant difference in the determined mobility values even for samples with 0.32 μm thickness. This result has several implications to our experiments: (i) the asymptotic determination of the mobility from the logarithm photocurrent vs logarithm time plots gives acceptable values even when the photocurrent transients are strongly dispersive; (ii) it was suggested that the morphology of solution cast films might vary with film thickness due to, for example, the different morphologies of concentrated solutions or the slower solvent evaporation of thicker films.[14,25]

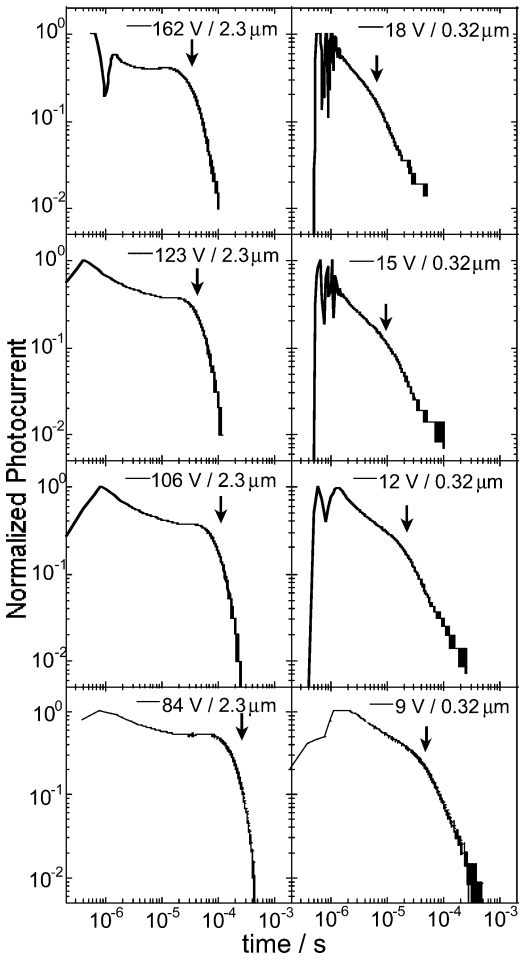

Figure 3. Log photocurrent vs log time plots of the photocurrent transients recorded for a 2.3 μm (left side) and a 0.32 μm (right side) RRa-MDMO−PPV device at various applied electric fields. The arrows indicate the meeting points of the two asymptotic linear regimes defined as the transit time of charge carriers.

Our results of thickness independent mobility suggest that the film morphology using the doctor blade technique does not change significantly by changing the film thickness within 0.32−2.3 μm as far as charge carrier mobility is concerned.

The room-temperature mobility values measured at 5×10^5 V cm^{-1} electric field have been determined and are summarized in Table 1. Several factors may be responsible for the improved charge transport property of 70:30 RS-MDMO−PPV. It was shown that chemical modifications of the conjugated polymer could change the electronic and morphologic properties in a complicated way. For instance, Veres et al. have reported that decreasing the amount of polymerization defects in PPV derivatives, the room-temperature mobility determined by the time-of-flight technique is increased.[23] Moreover, the work of Martens et al. compared the mobility values determined from space charge limited current measurement of three fully conjugated PPV copolymers as well as a partially conjugated PPV.[18] By measuring the electric field and temperature dependence of the mobility, they correlated the microscopic transport properties of the PPV copolymers with their molecular structure. It was reported that the broken conjugation decreases the mobility significantly. On the other hand, mobility of the fully conjugated polymers was found to be governed by the amount of energetic disorder related to the regularity of the conjugated chain and ordering in the solid phase.

Figure 4A,B shows the plot of logarithm mobility versus square root of electric field determined at several temperatures

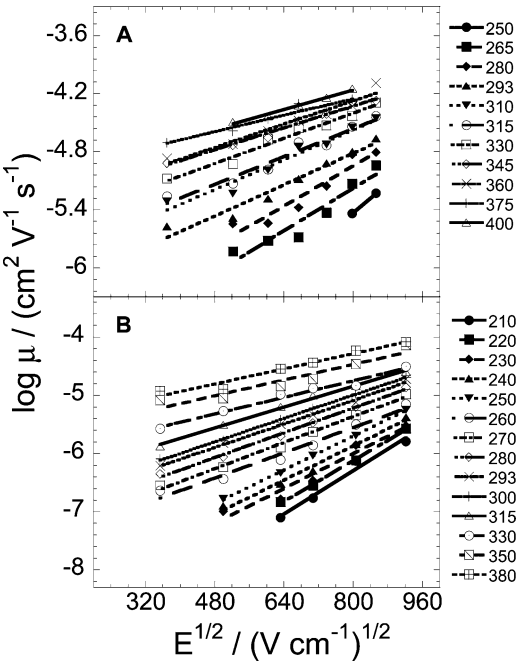

Figure 4. Electric field dependence of mobility of 70:30 RS-MDMO−PPV (A) and RRa-MDMO−PPV (B) at various temperatures. The lines represent linear fits of the data.

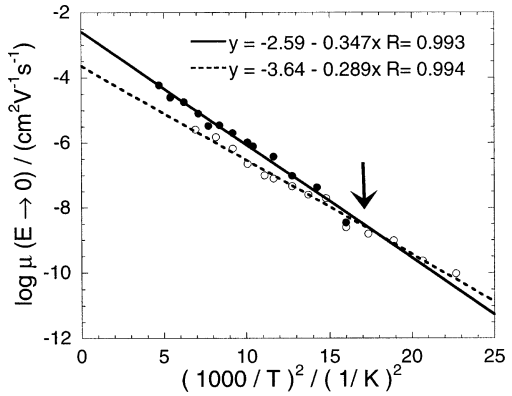

Figure 5. Temperature dependence of the zero field mobility of (●) 70:30 RS-MDMO−PPV and (○) RRa-MDMO−PPV. The lines and corresponding equations represent linear fits of the data.

for 70:30 RS-MDMO−PPV and RRa-MDMO−PPV, respectively. The slope of the field dependence of mobility is decreasing, and the zero field mobility (the mobility extrapolated to zero electric field) is increasing with increasing temperature. Such a tendency is predicted by the theory of disorder formalism introduced earlier.[11] Figure 5 shows the temperature dependence of the zero field mobility. The ordinate intercept of the lines obtained by a linear fit of the data determines the value of prefactor mobility, meanwhile the slope is related to the width of the Gaussian distribution of density of states. Figure 6 shows the slope of the field dependence versus $\sigma/(kT)$.[2] Figures 5 and 6 show that our experimental data can be fitted satisfactory using eq 1, and the disorder formalism may provide a framework for further discussion of the charge transport properties of these MDMO−PPV copolymers within the measured temperature range.

The calculated microscopic transport parameters derived from eq 1 are summarized in Table 1. The prefactor mobility is 1 order of magnitude higher for 70:30 RS-MDMO−PPV (sample 1), and the energetic disorder parameter also increases slightly. Interestingly, the zero field mobility of 70:30 RS-MDMO−PPV is only higher above ∼230 K but decreases faster due to the larger energetic disorder and eventually is lower than that of RRa-MDMO−PPV below 230 K, indicated by the arrow in Figure 5. Furthermore, the field dependence of mobility characterized by parameter C is slightly larger for the 70:30 RS-MDMO−PPV. The determined value of C agrees well within a factor of only 2 with the theoretically calculated value ($C = 2.9 \times 10^{-4}$ [(cm $V^{-1})^{1/2}$]), which further justifies the applicability of eq 1 to describe our experimental data.

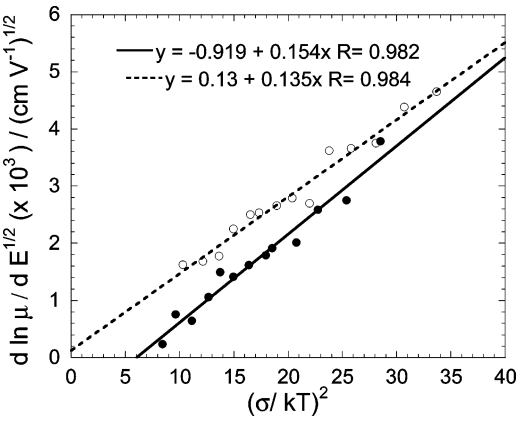

Figure 6. Slope of the field dependence against $(\sigma/kT)^2$, the energetic disorder parameter of eq 1, of (●) 70:30 RS-MDMO−PPV and (○) RRa-MDMO−PPV. The lines and corresponding equations represent linear fits of the data.

The prefactor mobility is primarily governed by the amount of electronic coupling between neighboring transport sites,[18] reflecting the magnitude of electronic wave function overlap, which is a sensitive function (exponential) of the intersite distance. Our results are rather surprising when compared to previous work of Martens et al.[18] The authors argued that the less configurational and conformational freedom of individual chains of their regioregular conjugated polymer (OC**10**C**10**−PPV) decreases the fluctuation of hopping site energies, thus lowering the intrachain energetic disorder. We propose that the slight increase of the energetic disorder of our regioregular copolymer may result from lower lying energy states of ordered nanoaggregates as compared to the amorphous matrix acting as energetic traps for overall charge transport. The above model is schematically illustrated in Scheme 2A,B. Scheme 2A illustrates charge motion in the amorphous regions of the films, in which the energies of the transport sites (polaron energy) experience a statistically varying environment, giving rise to a Gaussian distribution of density of states. Scheme 2B, on the other hand, depicts regions where the conjugated chains are partially aligned with a better interchain interaction. These regions are expected to create preferential paths ("highways") for the charge carriers, therefore increasing the mobility. In the framework of disorder formalism, on the other hand, the major source of disorder of the charge transport sites is assumed to originate from the variations of dipole−induced dipole interactions between the charge carrier and the surrounding polarizable matrix.[14] Because more interacting delocalized π-electron systems of the ordered regions are thought to be more polarizable, the extent of the dipole−induced dipole interactions is expected to be higher in the ordered regions of the films, which lowers the site energy. Because the ordered regions in our model are embedded in an amorphous matrix, these lower lying energy states may act as traps and broaden the density of states. Charge hopping at the end of these "highways" (indicated by the large arrow in Scheme 2B) requires sufficient thermal energy and/or tilting the barrier by an external electric field. Therefore, at high

SCHEME 2: Schematic Illustration of Charge Motion and the Energy of Hopping Sites (Polaron Energy): (A) When the Conjugated Chains Are Randomly Oriented; (B) When Local Ordering of the Conjugated Chains Takes Place

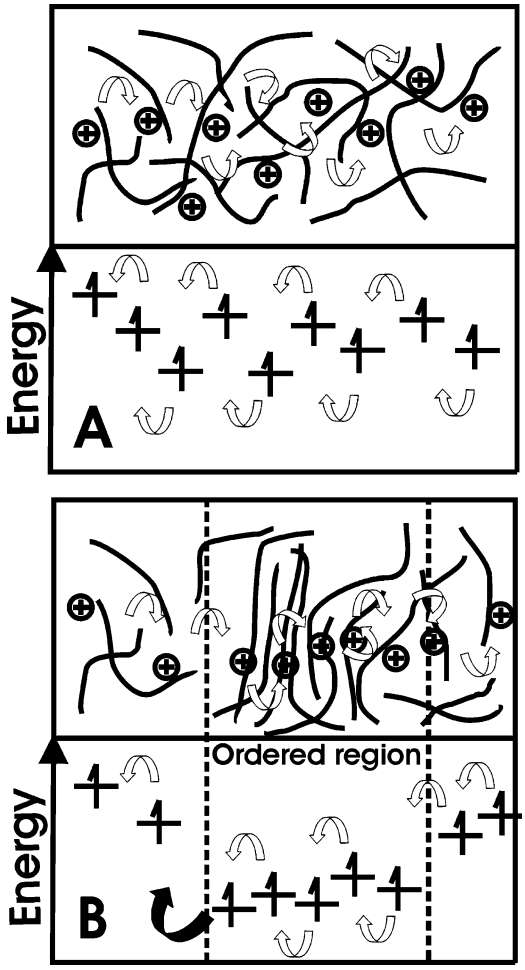

temperatures and high electric fields, films of 70:30 RS-MDMO−PPV with better interchain packing shows a higher charge carrier mobility. At low temperatures and low electric fields, however, charges might be trapped at the lower lying energy sites of the aligned regions, hence causing stronger temperature and electric field dependence of mobility. On the basis of the above model, it is emphasized that three-dimensional ordering, when it would spread over the entire bulk, is expected to increase the mobility significantly. However, in partially ordered cases when the ordered nanodomains are embedded in an amorphous matrix, the competitive interplay between increased energetic disorder and improved charge transport within these ordered regions is expected to control the charge carrier transport.

Numerous studies have revealed that interchain interactions are important in alkoxy-substituted PPVs,[25−31] and particularly in MDMO−PPV.[29,30] It has been reported that films with increased interchain interactions show a red shift of the luminescence bands, and characteristic enhancement of spectral features superimposed on the 0−1 and 0−2 vibronic sideband emission of the isolated intrachain exciton.[25,27,28] These features have been attributed to the radiative decay of interchain excitons and are highly indicative for the existence of aggregates.[28,31]

In Figure 7 the normalized photoluminescence spectra of films of 70:30 RS-MDMO−PPV and RRa-MDMO−PPV are compared. The spectral features between 620 and 750 nm show the

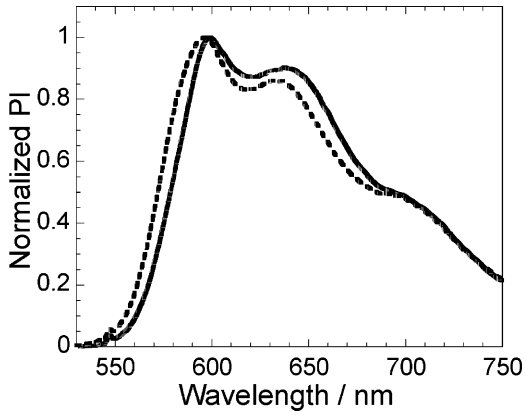

Figure 7. Normalized photoluminescence spectra of (—) 70:30 RS-MDMO−PPV and (- - -) RRa-MDMO−PPV films, prepared by the doctor blade technique from 1 wt % chlorobenzene solution.

presence of interchain species in both polymers. However, the features of the films of 70:30 RS-MDMO−PPV are red-shifted and slightly enhanced as compared to RRa-MDMO−PPV, which indicates the existence of more aggregated interchain species, in accordance with the conclusion of our charge transport studies. A more detailed characterization, including low temperature photoluminescence and thermally stimulated luminescence, will be published.

4.3. Photovoltaic Device Performance. We have prepared bulk heterojunction solar cells in order to utilize the improved charge transport properties of the novel regiospecific MDMO−PPV copolymer. The current density vs voltage curve of a bulk heterojunction solar cell based on the 1−4 ratio by weight mixture of the 70:30 RS-MDMO−PPV copolymer with the fullerene acceptor PCBM is compared with RRa-MDMO−PPV in Figure 8A,B, and the parameters characterizing the photovoltaic performance are summarized in Table 2. The current density vs voltage curve of the RRa-MDMO−PPV was taken from ref 1, and represents the state-of-the-art photovoltaic device based on the RRa-MDMO−PPV:PCBM blend. The active layers of both devices were approximately 100 nm thick, and great care was taken to prepare the 70:30 MDMO−PPV based devices in exactly the same manner as reported in ref 1. Although the short-circuit current and the open-circuit voltage are quite similar for the two devices, the bulk heterojunction solar cell based on 70:30 RS-MDMO−PPV has a higher power conversion efficiency of 2.65% under simulated AM 1.5 conditions due to the very high (0.71) filling factor.

We performed a mathematical simulation of the current density vs voltage curves shown in Figure 8 B based on the simple one-diode equivalent circuit model in the form of eq 4.[32]

$$J = J_0\left(\exp\left(\frac{V - JR_{RS}}{nk_BT}\right) - 1\right) + \frac{V - JR_{RS}}{R_R} - J_{SC} \quad \text{(A4)}$$

where J (A cm^{-2}) and V (V) are the current density and voltage values taken from Figure 8B, respectively, J_0 (A cm^{-2}) is the reverse bias dark current, R_s (Ω cm^{-2}) is the series resistance, R_p (Ω cm^{-2}) is the parallel resistance, and J_{sc} (A cm^{-2}) is the short-circuit current density under illumination. The equation has been numerically solved, and the parameters obtained by the best fit are summarized in Table 2. The factor of 2.3 lower series resistance together with the factor of 2.3 higher parallel resistance is responsible for the improved filling factor, and the improved photovoltaic performance of the 70:30 RS-MDMO−PPV based device. The factor of 2.3 times higher parallel

TABLE 2: Photovoltaic Performance of the Bulk Heterojunction Solar Cells, and the Parameters of Eq 4 Obtained by Numerical Calculation

mateial[a]	J_{sc} (mA cm^{-2})	V_{oc} (V)	FF	$\eta_{AM\ 1.5}$ (%)[b]	J_0 (mA cm^{-2})	R_s (Ω cm^{-2})	R_p (Ω cm^{-2})	n
1	5.0	0.8	0.71	2.65	6×10^{-7}	1.3	2150	1.9
2	5.25	0.82	0.61	2.5	6×10^{-7}	3	950	2.0

[a] Material 1 and 2 stands for 70:30 RS-MDMO−PPV: PCBM (1:4) and RRa-MDMO−PPV: PCBM (1:4), respectively. [b] Calculated using a value of mismatch factor $m = 0.753$, see text.

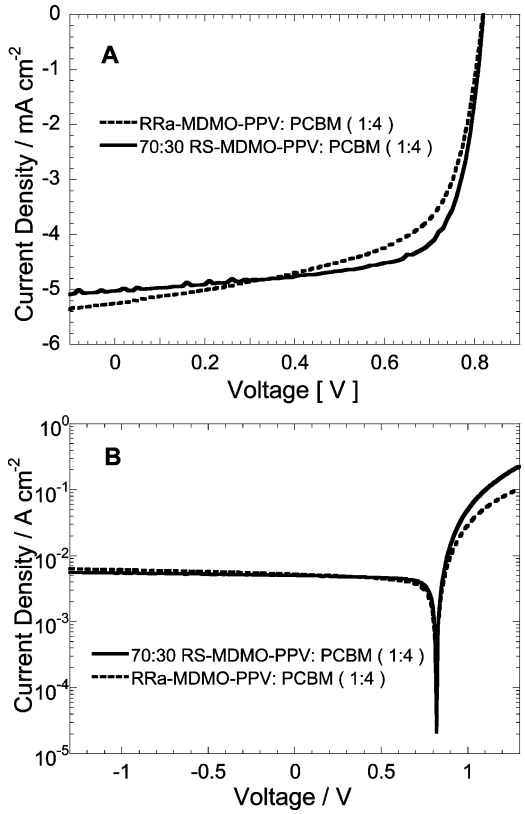

Figure 8. (A), (B) Current density vs voltage characteristics of bulk heterojunction photovoltaic devices based on 1:4 ratio by weight mixtures of (—) 70:30 RS-MDMO−PPV and (- - -) RRa-MDMO−PPV with PCBM. (B) shows the log current density versus applied voltage curves used for modeling the diode characteristics.

resistance most likely results from better film quality (e.g., less shunts and micro shorts). The factor of 2.3 times lower series resistance, on the other hand, can be related with an improved mobility of the photogenerated charge carriers in the photoactive blend of 70:30 RS-MDMO−PPV copolymer with PCBM. This result agrees well with the time-of-flight mobility data obtained for the pure 70:30 RS-MDMO−PPV; however the charge carrier mobility in an operational solar cell may be strongly influenced by the nanomorphology of the interpenetrating phases as well as the effect of charge carrier concentration due to trap filling effects under higher illumination intensities.

5. Conclusion

A regiospecific MDMO−PPV copolymer has been synthesized with improved charge transport properties by taking advantage of the sulfinyl precursor route. Analysis of the electric field and temperature dependence of the mobility reveals an interesting interplay between the 1 order of magnitude higher prefactor mobility and the increased disorder parameter of the regiospecific MDMO−PPV copolymer, as compared to the regiorandom counterpart. This phenomenon is attributed to the effect of partially ordered regions with increased interchain interactions embedded in an amorphous matrix: the better packing of the conjugated chains in the ordered regions facilitates enhanced charge transfer; however, the same ordered regions act as energetic traps for the charge carriers. At temperatures, when the surrounding thermal bath is sufficient to compensate for the larger energetic disorder effects (notably above 230 K), the higher prefactor mobility governs charge transport. Below 230 K, the effect of larger disorder dominates the charge transport properties. The improved charge transport properties of the novel regiospecific MDMO−PPV copolymer were used in fabrication of bulk heterojunction solar cells exhibiting an improved power conversion efficiency of 2.65% with high (0.71) filling factor.

Acknowledgment. This work was supported by the European Commission within the framework of the Human Potential-Research Training Network, EUROMAP" contract no. HPRN-CT-2000-00127, and was performed within the Christian Doppler Foundations dedicated Laboratory for Plastic Solar Cells funded by the Christian Doppler Foundation and Konarka Austria GmbH. The synthesis of the novel regiospecific MDMO-PPV was performed by the Limburgs Universitaire Centrum (LUC) and IMEC (IMOMEC division). We are also thankful for the support of Prof. Dr. Wolfgang Heiss with the PL setup and fruitful scientific discussions.

Supporting Information Available: Table 1S. Properties of the MDMO−PPV copolymers: weight averaged molecular weights and polymerization yields. This material is available free of charge via the Internet at http://pubs.acs.org.

References and Notes

(1) Brabec, C. J.; Sariciftci, N. S.; Hummelen, J. C. *Adv. Funct. Mater*. **2001**, *11*, 15.

(2) Shaheen, S. E.; Brabec, C. J.; Sariciftci, N. S.; Padinger, F.; Fromherz, T.; Hummelen, J. C. *Appl. Phys. Lett.* **2001**, *78*, 841.

(3) Brabec, C. J.; Cravino, A.; Meissner, D.; Sariciftci, N. S.; Fromherz, T.; Minse, M.; Sanchez, L.; Hummelen, J. C. *Adv. Funct. Mater*. **2001**, *11*, 374.

(4) Munters, T.; Martens, T.; Goris, L.; Vrindts, V.; Manca, J.; Lutsen, L.; De Ceuninck, W.; Vanderzande, D.; De Schepper, L.; Gelan, J.; Sariciftci, N. S.; Brabec, C. J. *Thin Solid Films* **2002**, *403*, 247.

(5) Geens, W.; Shaheen, S. E.; Brabec, C. J.; Poortmans, J.; Sariciftci, N. S. In *Electronic Properties of Novel Materials − Molecular Nanostructures*; Kuzmany, H., Fink, J., Mehring, M., Roth, S., Eds.; American Institute of Physics: New York, 2000; Vol. 544, pp 516−520.

(6) Pacios, R.; Bradley, D. D. C.; Nelson, J.; Brabec, C. J. *Synth. Met*. **2003**, *137*, 1469.

(7) Mihailetchi, V.; van Duren, J. K. J.; Blom, P. W. M.; Hummelen, J. C.; Janssen, R. A. J.; Kroon, J. M.; Rispens, M. T.; Verhees, W. J. H.; Wienk, M. M. *Adv. Funct. Mater*. **2003**, *13*, 43.

(8) Bao Z.; Dodabalapur, A.; Lovinger, A. J. *Appl. Phys. Lett.* **1996**, *69*, 4108.

(9) Sirringhaus, H.; Brown, P. J.; Friend, R. H.; Nielsen, M. M.; Bechgaard, K.; Langeveld-Voss, B. M. W.; Priering, A. J. H.; Janssen, R. A. J.; Meijer, E. W.; Herwig, P.; de Leeuw, D. M. *Nature* **1999**, *401*, 685.

(10) Lutsen, L.; Adriaensens, P.; Becker, H.; van Bremen, A. J.; Vanderzande, D.; Gelan, J. *Macromolecules* **1999**, *32*, 6517.

(11) Bässler, H. *Phys. Status Solidi B* **1993**, *175*, 15.

(12) Schein, L. B. *Phys. Rev. B* **1977**, *15*, 1024.

(13) Gelinck, G. H.; Warman, J. M.; Staring, G. J. *J. Phys. Chem.* **1996**, *100*, 5485.

(14) Bässler, H. In *Semiconducting Polymers: Chemistry, Physics and Engineering*; Hadziioannou, G., van Hutten, P. F., Eds.; Wiley VCH: Weinheim 2000.

(15) Menon, R.; Yoon, C. O.; Moses, D.; Heeger, A. J. In *Handbook of Conductive Polymers*, 2nd ed.; Skotheim, T. A., Elsenbaumer, R. L., Reynolds, J. R., Eds.; Marcel Dekker: New York 1998; pp 32−33.

(16) Borsenberger, P. M.; Weiss, D. S.; in Organic Photoreceptors for Imaging Systems; Marcel Dekker Inc.: New York, 1993.

(17) Shirota, Y. *J. Mater. Chem.* **2000**, *10*, 1.

(18) Martens, H. C. F.; Blom, P. W. M.; Schoo, H. F. M. *Phys. Rev B* **2000**, *61*, 7489.

(19) Im, C.; Bässler, H.; Rost, H.; Hörhold, H. H. *J. Chem. Phys.* **2000**, *113*, 3802.

(20) Miller, A.; Abrahams, E. *Phys. Rev.* **1960**, *120*, 745.

(21) Lutsen, L.; van Breemen, A. J.; Kreuder, W.; Vanderzande, D.; Gelan, J. *Helv. Chem. Acta* **2000**, *83*, 3113.

(22) van Breemen, A. J. J. M.; Vanderzande, D. J. M.; Adriaensens, P. J.; Gelan, J. M. J. V. *J. Org. Chem.* **1999**, *64*, 3106.

(23) Veres, J.; Becker, H.; Spreitzer, H.; Vestweber, H.; Kreuder, W. In *IS&T's NIP16: International Conference on Digital Printing Technologies*; IS&T: Vancouver, 2000; p 335.

(24) Sommeling, P. M.; Rieffe, H. C.; van Roosmalen, J. A. M.; Schonecker, A.; Kroon, J. M.; Wienke, J. A.; Hinsch, A. *Solar Energy Mater. Solar Cells* **2000**, *62/4*, 399.

(25) Shi, Y.; Liu, J.; Yang, Y. *J. Appl. Phys.* **2000**, *87*, 4254.

(26) Kadashchuk, A.; Skryshevski, Y.; Piryatinski, Y.; Vakhnin, A.; Emelianova, E. V:; Arkhipov, V. I.; Bässler, H.; Shinar, J. *J. Appl. Phys.* **2002**, *91*, 5016.

(27) Nguyen, T.-Q.; Doan, V.; Schwartz, J. B. *J. Chem. Phys.* **1999**, *110*, 4068.

(28) Nguyen, T.-Q.; Martini, I. B.; Liu, J.; Schwartz, B. J *J. Phys. Chem. B* **2000**, *104*, 237.

(29) Kemerink, M.; van Duren, J. K. J.; Jonkheijm, P.; Koenraad, P. M.; Janssen, R. A. J.; Salemink, H. W. M.; Wolter, J. H. In *Organic and Polymeric Materials and Devices*; Blom, P. W. M., Greenham, N. C., Dimitrakopoulos, C. D., Frisbie, C. D., Eds.; Material Research Society: Warrendale, PA, 2003; Vol. 771, pp 23−28.

(30) Gelinck, G. H.; Warman, J. M.; Staring, E. G. J. *J. Phys. Chem.* **1996**, *100*, 5485.

(31) Ho, P. K. H.; Kim, J.-S.; Tessler, N.; Friend, R. H. *J. Chem. Phys.* **2001**, *115*, 2709.

(32) Sze, S. M. In *Physics of Semiconductor Devices*; Wiley-Interscience: New York, 1981; p 806.